Molecular dynamics simulation of nanochannel flows with effects of wall lattice-fluid interactions

C. Y. Soong*
Department of Aerospace and Systems Engineering, Feng Chia University, Seatwen, Taichung 40724, Taiwan, Republic of China

T. H. Yen
Graduate School of Defense Science Studies, Chung Cheng Institute of Technology National Defense University, Tahsi, Taoyuan 33509, Taiwan, Republic of China

P. Y. Tzeng
Department of Aeronautical Engineering, Chung Cheng Institute of Technology, National Defense University, Tahsi, Taoyuan 33509, Taiwan, Republic of China

(Received 28 March 2007; published 11 September 2007)

In the present paper, molecular dynamics simulations are performed to explore the effects of wall lattice-fluid interactions on the hydrodynamic characteristics in nanochannels. Couette and Poiseuille flows of liquid argon with channel walls of face-centered cubic (fcc) lattice structure are employed as the model configurations. Truncated and shifted Lennard-Jones (LJ) 12-6 potentials for evaluations of fluid-fluid and wall-fluid interactions, and a nonlinear spring potential for wall-wall interaction, are used as interatomistic or molecular models. The hydrodynamics at various flow orientation angles with respect to channel walls of lattice planes (111), (100), and (110) are explored. The present work discloses that the effects of key parameters, such as wall density, lattice plane, flow orientation, and LJ interaction energy, have a very significant impact on the nanochannel flow characteristics. The related interfacial phenomena and the underlying physical mechanisms are explored and interpreted. These results are significant in the understanding of nanoscale hydrodynamics, as well as in various applications where an accurate nanoscale flow rate control is necessary.

DOI: 10.1103/PhysRevE.76.036303 PACS number(s): 47.61.Fg, 47.27.nd, 47.11.Mn

I. INTRODUCTION

Compared with flow at conventional conditions, fluid flows at nanoscales have remarkable differences in hydrodynamic characteristics. Interfacial phenomena such as fluid slippage at the wall-fluid interface are significant issues in investigations of nanofluidics. The so-called boundary slip can be classified in various respects, e.g., fluid truly sliding over solid surfaces, apparent slip stemming from surface inhomogeneities, and complex interfacial effects with additional physics, etc. At various wall and fluid conditions, the behaviors of slip, no-slip, and multilayer locking have been observed [1]. Molecular dynamics (MD) simulation is an appropriate approach used widely for dealing with detailed interfacial phenomena. Simple flows, such as the Couette and Poiseuille flows in narrow channels with widths of a few molecular diameters, are the most common configurations chosen for MD simulations of nanofluidics. Interesting physical behaviors, such as density layering phenomena and fluid slippage, have been demonstrated in a number of previous MD simulations.

At nanoscales, the interfacial phenomena and fluid behaviors are strongly influenced by the surface conditions of the solid wall. Some previous studies focused on the effects of wall-fluid interaction parameters. For example, Thompson and Robbins [2] and Thompson and Troian [3] changed the solid-fluid interaction energy parameter and wall density to study their effects on the slip length. Using MD simulation of thin films of hexadecane, slip characteristics on absorbing surfaces under various conditions were explored [4]. Many studies, such as those of Barrat and Bocquet [5,6], Cottin-Bizonne *et al.* [7], Priezjev *et al.* [8], and Cieplak *et al.* [9], dealt with the influence of hydrophobicity or wettibility of the wall-fluid interface. For example, Barrat and Bocquet [5,6] modulated the wettability of the substrate by modulating the magnitude of the attractive force between particles. Soong *et al.* [10] performed MD simulations of a nanoscale rotating fluid in a cylindrical container and found nonlinear slip behavior different from that appearing in linear Couette flows, especially around the corner regions of the container.

Among the influential factors, the surface roughness is quite significant for interfacial phenomena. A roughened wall can be intentionally fabricated with elements mounted on or grooves indented in solid surfaces. A few previous studies dealt with the effects of surface obstacles or grooves in nanoscale flows, e.g., Couette flow [11] and electro-osmotic flow [12,13]. In addition, by using a lattice Boltzmann method, Sbragaglia *et al.* [14] studied roughness-hydrophobicity coupling in nanochannels with grooved surfaces. In these cases, the roughness elements considered were of several σ (molecular length scale) in height and width.

From a microscopic point of view, even when there is no artificial roughness on the channel walls, the lattice arrangement of wall atoms at the wall-fluid interface will produce roughness at the atomistic level. The distance or gap between two neighboring atoms may be of the order of 0.1–1 nm. In a nanochannel tens of nanometers in height, this class of surface roughness is expected to be influential in the fluid flow. The so-called lattice plane or surface orientation of a solid wall characterized by its Miller indices can be a control parameter in nanochannel flows. Considering the flow orien-

*Corresponding author. cysoong@fcu.edu.tw

 ©2007 The American Physical Society

tation with respect to the lattice structure, the flow angle becomes another significant parameter. In the literature, one can find only a few studies on the effects of crystal-fluid interaction on material bulk properties and thermodynamics [15,16]. Galea and Attard [17] studied the effect of solid atomistic roughness on the slip length by changing the wall density of a fixed crystal plane, the face-centered cubic (fcc) (100) plane. They found a nonmonotonic trend of slip length variation with changes in wall density. However, the influence of the lattice plane on the fluid flows in nanochannels has not been investigated yet. Furthermore, the flow orientation with respect to the lattice structure has not been taken into account in previous investigations of nanoscale fluid flows.

The objective of the present study is to explore the effects of the wall crystal-fluid interactions in nanochannels by using molecular dynamics simulation. Couette and Poiseuille flows with channel walls of fcc lattice structure are employed as the model configurations. Truncated and shifted Lennard-Jones (LJ) potentials for evaluation of the fluid-fluid and the wall-fluid interactions, and a nonlinear spring potential for wall-wall interaction, are used. With liquid argon of densities $\rho_{f,b}\sigma^3=0.81$ and 0.95 as the model fluid, various wall densities $\rho_w\sigma^3=1.0-4.0$ and wall-fluid interaction parameters $\varepsilon_{wf}/\varepsilon=0.4-1.0$ are considered. The hydrodynamics at various surface and flow orientation angles with respect to the channel walls of the surfaces fcc (111), (100), and (110) are explored.

II. METHODOLOGY

The channel-fluid system under consideration is composed of fluid molecules confined between two parallel planar walls separated with a height H. Both Couette and Poiseuille flows are investigated in the present study. Periodic boundary conditions are imposed on the upstream and downstream boundaries (X direction) and two sides (Y direction) of the computational domain of size $16\sigma\times16\sigma\times21.8\sigma$. Couette flow is a planar fluid layer with the upper wall moving at a constant velocity U_w along the streamwise direction (X), whereas in Poiseuille flow, an external force stemming from the pressure gradient f_p in the X direction is applied to the fluid particles. The position of the first layer of molecules in the solid lattice is set as the reference for the Z axis.

In this study, with emphasis on the interfacial phenomena and related physical mechanisms, a simple fluid commonly used in MD simulations, liquid argon, is employed as the model fluid. In addition, for convenience, we employ a hypothetical solid wall of fcc lattice structure with a nonlinear spring model of interaction between wall atoms. The details of the MD model are as follows.

A. Potential models

In the present MD simulations, the pair potential between fluid-fluid and fluid-wall atoms is governed by truncated and shifted Lennard-Jones potentials, viz.,

$$\phi_{\alpha\beta}(r_{ij})=\begin{cases}4\varepsilon_{\alpha\beta}\left[\left(\frac{\sigma_{\alpha\beta}}{r_{ij}}\right)^{12}-c_{\alpha\beta}\left(\frac{\sigma_{\alpha\beta}}{r_{ij}}\right)^{6}-\left(\frac{\sigma_{\alpha\beta}}{r_c}\right)^{12}+c_{\alpha\beta}\left(\frac{\sigma_{\alpha\beta}}{r_c}\right)^{6}\right], & r_{ij}\leqslant r_c,\\ 0, & r_{ij}>r_c,\end{cases} \tag{1}$$

where the parameters $\varepsilon_{\alpha\beta}$ and $\sigma_{\alpha\beta}$ are, respectively, the energy and length scales for the interaction of species α and β, and r_{ij} is the separation distance between the particles i and j. The Lorentz-Berthelot mixing rule is adopted to evaluate interaction parameters pertaining to two dissimilar species, i.e., $\varepsilon_{\alpha\beta}=\sqrt{\varepsilon_{\alpha\alpha}\varepsilon_{\beta\beta}}$ and $\sigma_{\alpha\beta}=(\sigma_{\alpha\alpha}+\sigma_{\beta\beta})/2$. The interaction parameters between solid and fluid particles are $\varepsilon_{wf}=\sqrt{\varepsilon_{ff}}$ with $\varepsilon_{ww}=1.0$ and $\sigma_{wf}=(\sigma_{ww}+\sigma_{ff})/2$. In the following text, the fluid-fluid parameters ε_{ff} and σ_{ff} are employed as the characteristic molecular energy and length scales. The parameter $c_{\alpha\beta}$ is the coefficient of the attraction term. For common LJ fluids, the coefficient $c_{ff}=1.0$ [2,3] is defined, while for a more cohesive LJ fluid, c_{ff} has a higher value, e.g., $c_{ff}=1.2$ [4,5]. In the present study, these two kinds of interactions between fluid atoms are both considered. For comparison, we consider the special case of $c_{ff}=0$, which corresponds to the so-called Weeks-Chandler-Anderson (WCA) model with attraction ignored [18]. To save computational time, as in the usual MD simulations in previous work, a cutoff distance r_c is chosen for each model, beyond which the intermolecular forces are neglected for the small interactions between molecules at relatively large distances. The cutoff distance is $r_c=2.5\sigma$ for the usual LJ flow, and $r_c=2.8\sigma$ for the more cohesive LJ flow. For comparison, we also perform a few computations using the WCA model, whose cutoff distance is $r_c=\sqrt[6]{2}\sigma$. The mass of wall atoms is assumed to be identical to that of the fluid atoms. The wall-fluid interaction potential ϕ_{wf} has a similar form as Eq. (1) but with the parameters denoted by ε_{wf}, σ_{wf}, and c_{wf}, where $c_{wf}=1.0$.

Liquid molecules are initially arranged at the lattice sites, and the walls are composed of four layers of atoms fixed as a face-centered cubic lattice structure. Each wall atom may oscillate about its lattice site; a nonlinear spring potential for a fcc lattice,

$$\phi_{ww}(S)=(H_1/2)S^2+(H_1/4d_{cr}^2)S^4+(H_1/6d_{cr}^4)S^6, \tag{2}$$

is employed, in which the parameters H_1, H_2, and H_3 are the spring constants; S stands for the displacement of a wall

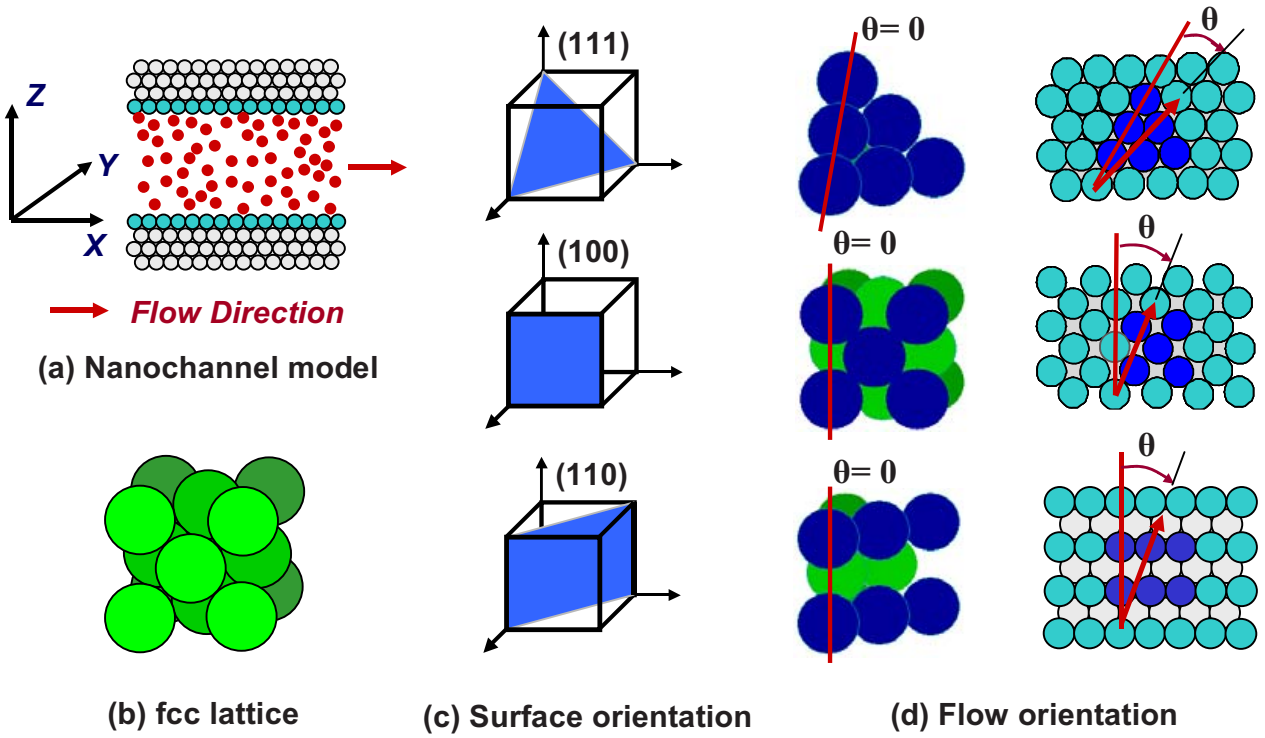

FIG. 1. (Color online) Flow channel models, surface orientation, and flow orientation. (a) Nanochannel model; (b) face-centered cubic crystal lattice; (c) surface orientation or crystal plane; (d) flow orientation.

molecule from its lattice site; and the parameter d_{cr}^2 is the critical mean-square displacement of the wall atom, which is determined according to the Lindemann criterion for melting, $d_{cr}^2 < 0.023R_0^2$. We use $d_{cr}^2 = 0.01R_0^2$, where R_0 is the nearest-neighbor distance. The density of the solid wall can be expressed as $\rho_w = 4/a^3$, where a is the unit cell length. The equilibrium nearest-neighbor spacing R_0 can be expressed as $a/\sqrt{2}$. The LJ length scale of wall atoms, σ_{ww}, can be evaluated by the following relation [17]:

$$\sigma_{ww} = R_0/1.09. \tag{3}$$

The roughness of the solid surface alters with the unit cell length a, and, therefore, the interaction length scale of the wall molecules, σ_{ww}, is changed. With the length parameters of the fluid molecules and wall atoms, σ_{ff} and σ_{ww}, the wall-fluid interaction length scale σ_{wf} can be evaluated according to the Lorentz-Berthelot mixing rule $\sigma_{wf} = (\sigma_{ww} + \sigma_{ff})/2$.

B. Thermostat

Khare *et al.* [19] compared two approaches for keeping the system temperature constant, one with thermostat applied only to the wall atoms and the fluid particles within the thin layer closest to the walls, and the other with the thermostat applied to the molecules in the entire fluid region. Based on their results, the former thermostat was recommended. In the investigation of Hagen-Poiseuille flow through a cylindrical pore, Heinbuch and Fischer [1] disclosed that the flow pattern depends on the wall-fluid interaction, the driving force, the treatment of the thermostat, and the thermodynamic state. To attain the statistical formalism of the ensemble, the Nosé-Hoover thermostat [20] is adopted. For the fluid particles adjacent to the walls, since there are only a few fluid particles within the near-wall region of width 0.5σ, the thermostat is actually applied to the particle motion in the Y direction within an outer layer of $Y = (0.6-1.1)\sigma$. For the solid wall, a three-directional Nosé-Hoover thermostat is adopted.

C. Governing parameters in simulations

In the present study, the fluid-fluid interaction energy ε_{ff} and length σ_{ff}, the conventional molecular units, are taken as the molecular energy and length scales, and the notations ε and σ are used for brevity. The notation m stands for the mass of the molecule, σ for the length scale, ε for the energy scale, $\tau = (m\sigma^2/\varepsilon)^{1/2}$ for the time scale, and ε/k_B for the temperature scale. For liquid argon, the scales are $\sigma = 3.405$ Å, $\varepsilon = 119.8k_B$, and $\tau \simeq 2.2 \times 10^{-12}$ s. The dimensions of density, velocity, force, and viscosity are σ^{-3}, σ/τ, ε/σ, and $\varepsilon\tau/\sigma^3$, respectively. The Newtonian equation of motion of the molecules is integrated by using a velocity Verlet algorithm with a time step of $3 \times 10^{-3}\tau$. In previous work [3], it is claimed that, in the case of $U_w = 1.0\sigma/\tau$, the time periods of 100τ for stabilization and 200τ for data sampling and averaging are required to reduce thermal fluctuations. In the present study, the time period of 300τ for each simulation is sufficient to reach this end.

In the present flow model, the channel height $H = 21.8\sigma$, the numbers of fluid atoms $N_f = 4301$ or 5112, the numbers of wall atoms $N_w = 1120-2896$, the wall densities $\rho_w\sigma^3 = 1.0-4.0$, the fluid densities $\rho_{f,b}\sigma^3 = 0.81$ and 0.95, the temperatures $k_BT/\varepsilon = 1.0$ and 1.1, and the viscosities $\mu\sigma^3/\varepsilon\tau$

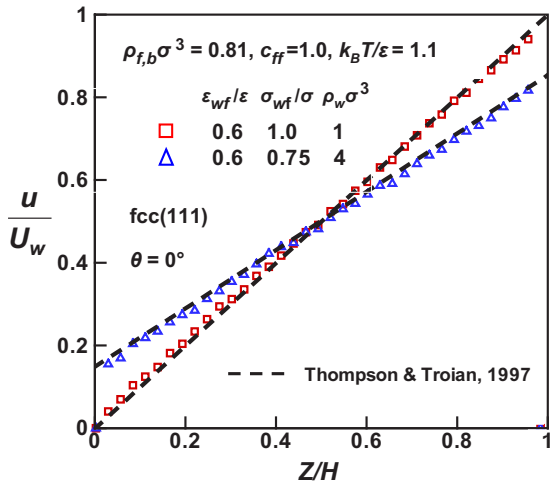

FIG. 2. (Color online) Verification of the simulation by comparison of the present results with the previous MD results [3] for Couette flow in a nanochannel of the fcc (111) wall surface.

=2.14 for liquid Ar and about 5 for a more cohesive fluid are considered. The interaction energy ε_{wf} spans from 0.4 to 1.0, and ε_{wf}=1.0 is used if not specified. The interaction length scale σ_{wf} is calculated based on the Lorentz-Berthelot mixing rule as mentioned in Sec. II A.

Three surface orientations, fcc (111), fcc (100), and fcc (110), are considered. Both surfaces (111) and (100) have closely packed atomistic structures and small distances between neighboring atoms; whereas the lattice plane (110) has a relatively sparse structure with atomistic trenches appearing in the first layer of atoms which contact the fluid particles. Among these three surface orientations, the plane fcc (111) is the smoothest, fcc (110) is the roughest, and fcc (100) lies in between. In addition, wall-fluid interactions in the presence of various flow orientations with respect to the crystal plane are explored. Figure 1(a) shows the nanochannel model; Fig. 1(b) the fcc lattice structure; Fig. 1(c) the lattice planes or surface orientations; and Fig. 1(d) the definition of the flow orientation angle and the global view of the surface and flow orientations.

III. RESULTS AND DISCUSSION

Before simulations for systematic study, the validation of the present MD simulation was examined. Figure 2 presents a comparison of the present with the previous results [4], in which only fcc (111) was studied. Basically, our simulations agree quite well with the previous ones. This demonstrates the appropriateness of the present MD simulation code.

A. Density profiles

In Fig. 3(a), a typical example of density layering phenomenon associated with nanoscale fluid behavior is presented. The fluid density is oscillatory in the near-wall region and meets the bulk fluid density in the off-wall core region. Figures 3(b)–3(e) show closeup views of near-wall density profiles in Couette flows with various surface and flow orientations. It is observed from the results at θ=0° in Fig. 3(b)

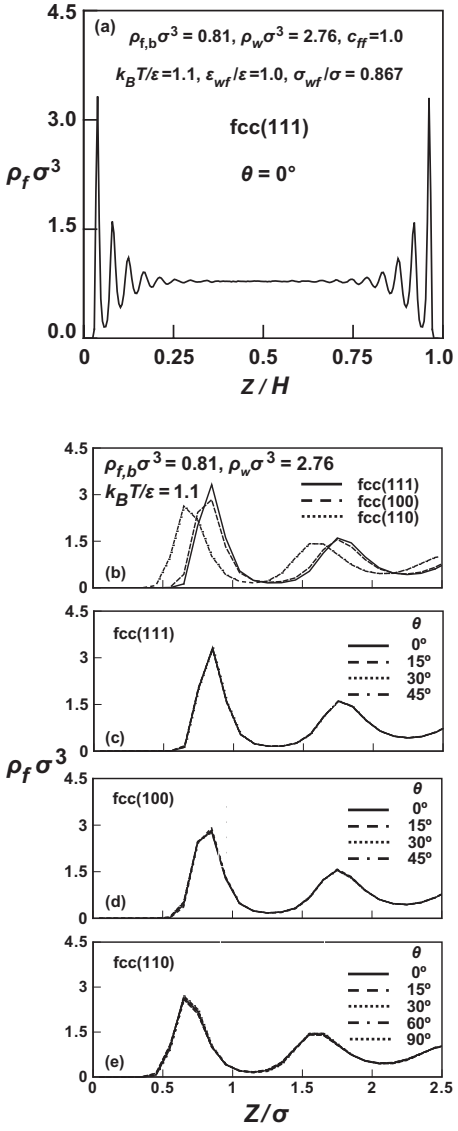

FIG. 3. Effects of lattice plane and flow orientation on fluid density distributions. (a) Typical density distribution; (b) effects of lattice plane; (c)–(e) effects of flow orientation.

that the density profiles for the two closely packed lattice planes, (111) and (100), are very similar, both qualitatively and quantitatively. The relatively sparse one, (110), however, has peaks a little lower and locations closer to the wall. In the case of lattice plane (110), a relatively stronger momentum and energy exchange between wall and fluid atoms occurs, and the fluid atoms reflect from the wall with less momentum and energy, which causes the locations of the density peaks to move toward the wall. This demonstrates the influence of the wall lattice plane. The data presented in Figs. 3(c)–3(e) disclose that the flow orientation has little influence on the density profiles. It can be elucidated that the density layering is a consequence of interactions between wall and fluid particles even when the bulk fluid is stationary. Therefore, the density layering is regarded as a fluid static feature in the sense of bulk flow; it has little relation to the flow direction.

To explore the influences of the wall-fluid interaction parameters, the near-wall density profiles at various conditions

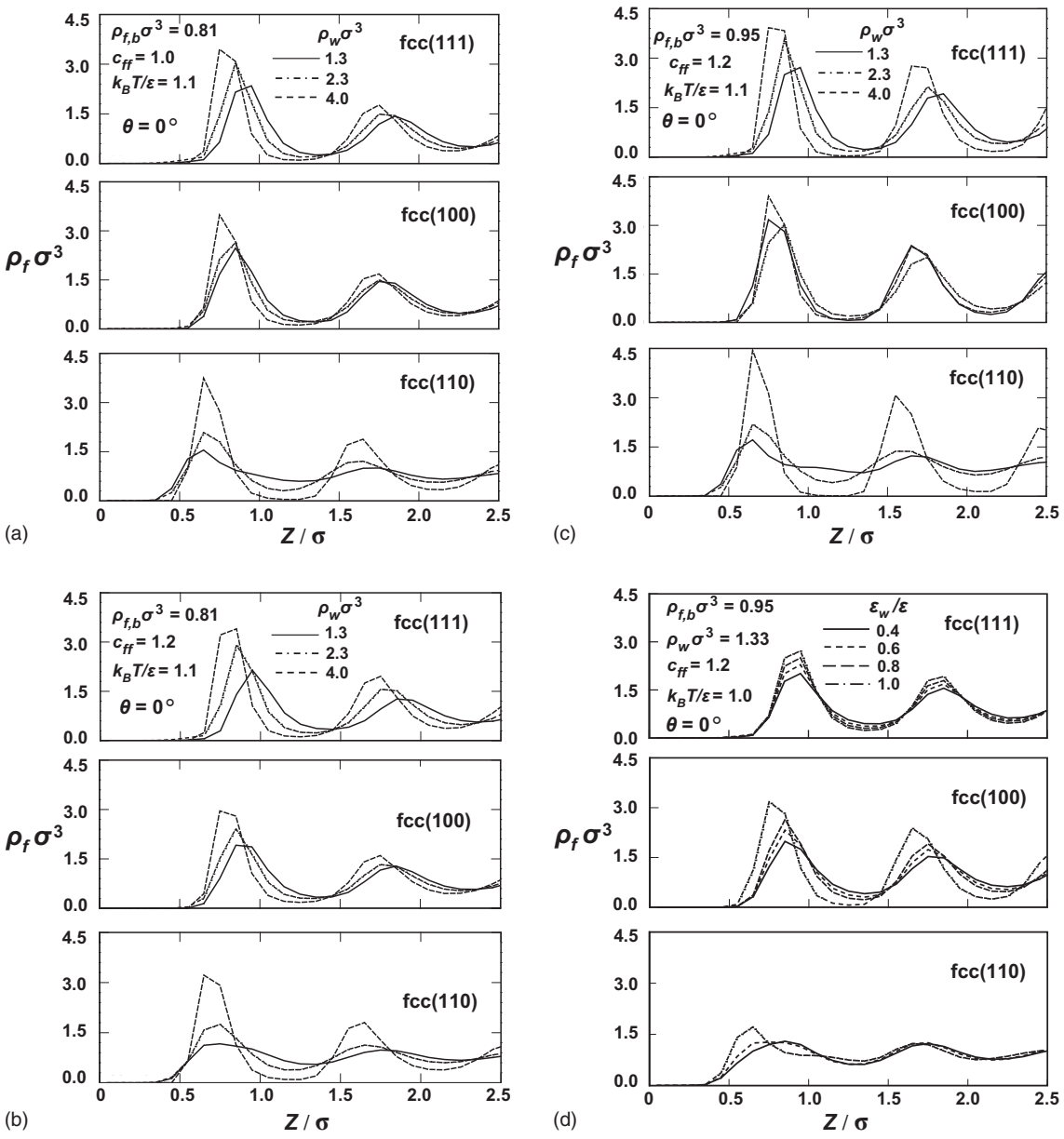

FIG. 4. Near-wall density profiles at flow orientation angle θ=0° under various conditions.

are shown in Fig. 4, where the results with $\rho_{f,b}\sigma^3$=0.81, c_{ff} =1.0, k_BT/ε=1.1, $\varepsilon_{wf}/\varepsilon$=1.0, and $\rho_w\sigma^3$=1.3–4.0 are presented in Fig. 4(a) for reference. Generally, the results shown in Fig. 4 reveal that a higher wall density leads to more remarkable density layering phenomenon, with enhancement of the peak values as well as shift of the peak locations toward the wall. Compared with the baseline cases in Fig. 4(a), change in c_{ff} results in little change as shown in Fig. 4(b). It can be observed that, in Figs. 4(b) and 4(c), increase in fluid density and reduction in fluid temperature both increase the level of the fluid density. The effects of the interaction parameter ε_{wf} on the density layering phenomenon at $\rho_w\sigma^3$=1.3 are presented in Fig. 4(d). Increase in the wall-fluid interaction parameter $\varepsilon_{wf}/\varepsilon$ implies an enhanced energy exchange between wall and fluid, and, in turn, the data show that the density peaks are pronounced and their locations shifted toward the wall. For the most roughened case, fcc (110), the density layering is weaker.

Figure 5 presents quantities for characterizing the density layering phenomenon, i.e., the amplitude $A_p \equiv \rho(Z_p)/\rho_{f,b}$ and the location Z_p of the first peak in the density profile. In Fig. 5(a), the rough surface fcc (110) has monotonically increasing amplitude A_p as the wall density increases; while for the two relatively smoother surfaces, fcc (111) and (100), A_p presents different behaviors, and, especially, a nonmonotonic trend appears in the range of $\rho_w\sigma^3$ around 3. The reason for this nonmonotonic variation of A_p can be addressed as follows. The density oscillation can be enhanced with an increase in wall density but, at the same time, the characteristic length or influence range of the wall-fluid interaction σ_{wf} decreases with increasing $\rho_w\sigma^3$. These two counter effects may make the change in A_p nonmonotonic. For the more cohesive fluid with c_{ff}=1.2, as shown in Fig. 5(b), the same trend is obtained. For comparison, simulations with the WCA model (c_{ff}=0) are plotted, and the predictions reveal

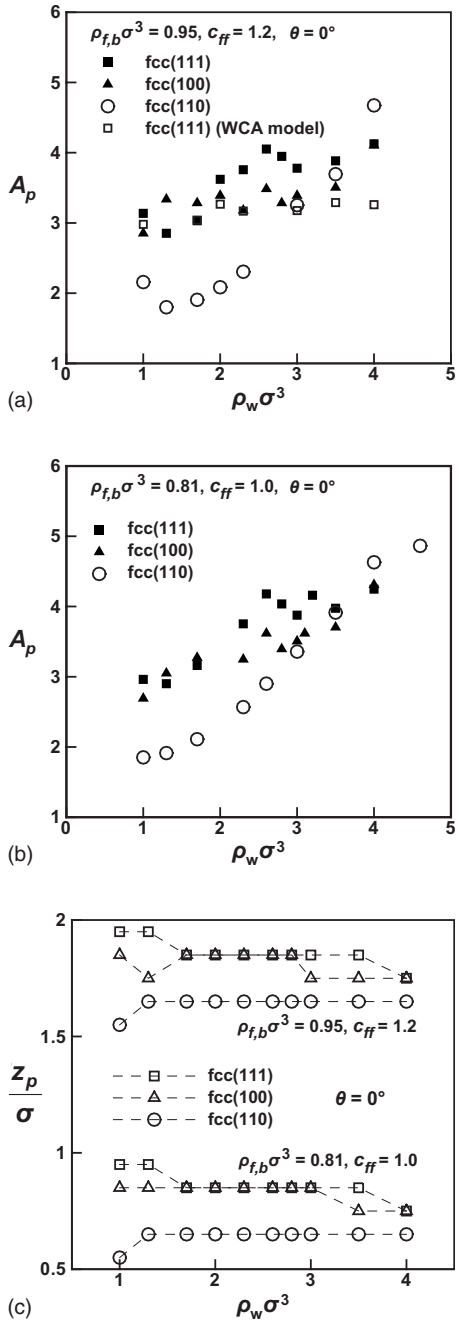

FIG. 5. First density peak A_p of the fluid density distribution in (a) usual LJ fluid (c_{ff}=1.0) and (b) more cohesive LJ fluid (c_{ff} =1.2). (c) Locations of the peak A_p.

that, without accounting for the attractive force between molecules, the fluid density oscillation is little influenced by the wall density. The correlation of the location Z_p of the first density peak with $\rho_w\sigma^3$ is presented in Fig. 5(c). In general, the location of the density peak is not sensitive to the change in wall density, especially in the intermediate range of $\rho_w\sigma^3$, where the location of the first fluid density peak remains almost unchanged. The surface fcc (110) is of a more anisotropic nature and is rougher than the other two surface orientations. For the lattice plane fcc (110), the increments in A_p with increasing $\rho_w\sigma^3$ are larger than for the other two surfaces. This enhancement of the density layer phenomenon at

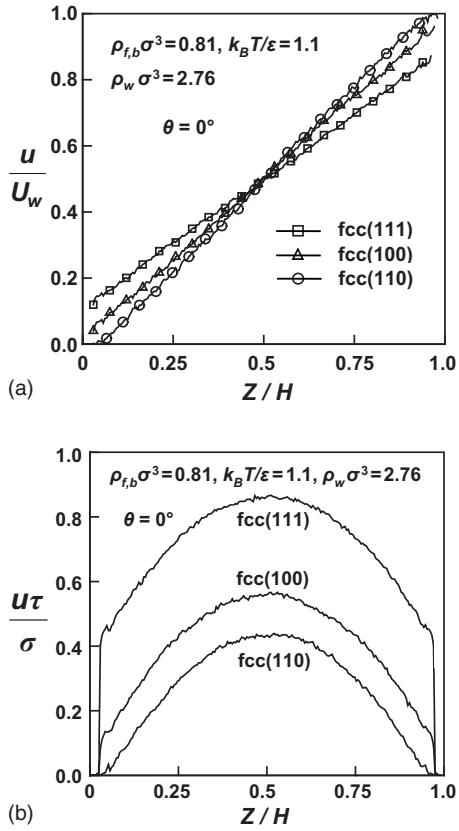

FIG. 6. Effects of lattice plane on flow velocity distributions at θ=0°, $\rho_w\sigma^3$=2.76, $\rho_{f,b}\sigma^3$=0.81, k_BT/ε=1.1. (a) Couette and (b) Poiseuille flow.

higher A_p is caused by the stronger influences of the second layer of wall atoms that are exposed in the trenches of first-layer structures, and also have the smallest distance from the first layer of wall-fluid particles. As the wall density increases, the density layering phenomenon becomes more pronounced with decreasing distance between the first and second layers of wall atoms.

B. Velocity profiles

Figure 6(a) shows the velocity profiles in the Couette flow with solid walls of various lattice planes but a fixed flow orientation angle θ=0°. The results reveal that the velocity distributions are basically linear, but distinct from each other in boundary slip. The most notable fluid slippage at the wall-fluid interface is that for the most packed surface (111), and least for the surface (100). The lattice plane (110) with atomistic trenches may trap fluid particles via strong wall-fluid interactions. This fact leads to a strong multilayer-sticking phenomenon characterized by a negative slip length. Figure 6(b) shows the MD predictions of the velocity distributions in the Poiseuille flow driven by a constant force f_p =0.02ε/σ. The velocity profiles for (111), (100), and (110) are of the same curve type but, similar to the observations on Couette flow, they deviate from each other in different degrees of fluid slippage appearing at the wall-fluid interface.

Each of the three fcc lattice planes considered in the present work has its own symmetric nature. This can be seen

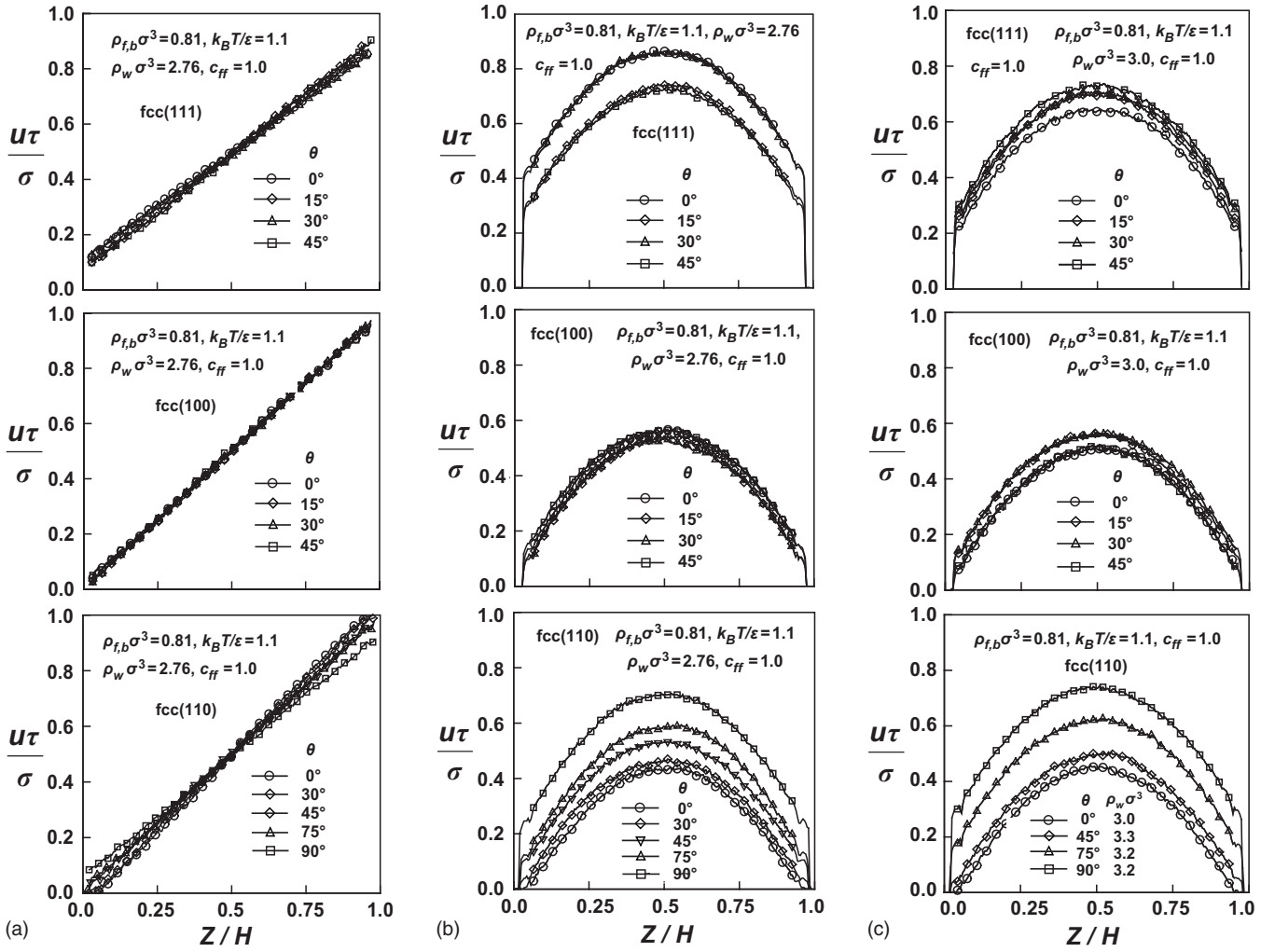

FIG. 7. Effects of flow orientation on (a) Couette and (b) Poiseuille flow velocity distributions at $c_{ff}=1.0$, $k_BT/\varepsilon=1.1$, $\rho_{f,b}\sigma^3=0.81$, and $\rho_w\sigma^3=2.76$; (c) Poiseuille flow velocity distributions at $c_{ff}=1.0$, $k_BT/\varepsilon=1.1$, $\rho_{f,b}\sigma^3=0.81$, and $\rho_w\sigma^3=3.0–3.3$.

from the surface (first-layer) atomistic pattern shown in Fig. 1. For the lattice plane (111), the first layer of atoms has a line of symmetry at $\theta=30°$, and flow orientations of $\theta=0°$, 15°, 30°, and 45° are explored. Similarly, the first layer of the (100) plane has a line of symmetry at $\theta=45°$, and flow orientations of $\theta=0°$, 15°, 30°, and 45° are studied. As to the plane (110), it is symmetric with respect to the line $\theta=90°$. There are parallel trenches of atomistic scale along the direction of $\theta=90°$; therefore, flow characteristics at the flow angles (θ) between 0° and 90° are simulated to examine the effects of flow orientation. Since the second and third layers of solid-wall atoms may also give contributions to the interfacial phenomenon, the distances between atomistic layers are also significant. Taking the wall density $\rho_w\sigma^3=2.76$ as an illustrative example, the distances between the neighboring layers of surfaces (111), (100), and (110) are, respectively, 1.1314σ, 0.9798σ, and 0.6928σ, which are within the range of the cutoff distance $\sigma_c=2.5\sigma$ in MD simulations. It implies that, in addition to the first layer, the wall atoms of the second and third layers will also have notable influences on the fluid particles near the interface. However, the wall atoms in the first layer contact the fluid directly and thus dominate the wall-fluid interactions.

The present MD predictions of velocity distributions demonstrate that this class of nanochannel flows can be significantly influenced by the flow orientation. Figures 7(a) and 7(b), respectively, show the Couette and Poiseuille flows of the usual LJ fluids with $c_{ff}=1.0$, $\rho_w\sigma^3=2.76$, $\rho_{f,b}\sigma^3=0.81$, and $k_BT/\varepsilon=1.1$. For both flows, the MD results reveal that, among the three lattice planes, the flow with a channel wall of surface (100) is most insensitive to the variation of the flow orientation. The most roughened and anisotropic surface (110) with flow orientation angles between 0° and 90° generates noticeable and monotonic effects on the flow field. Figure 7(c) presents the velocity profiles in the same conditions as above, but with the wall density increased up to $\rho_w\sigma^3=3.0–3.3$. Comparing Fig. 7(c) with Fig. 7(b), the hydrodynamic behaviors at $\rho_w\sigma^3=3.0–3.3$ are quite similar to those in the cases of $\rho_w\sigma^3=2.76$, but the fluid slippage and the flow orientation effects seem enhanced in the presence of higher wall density.

C. Slip length

The fluid slippage at the solid-liquid interface is an important hydrodynamic characteristic in dealing with nanos-

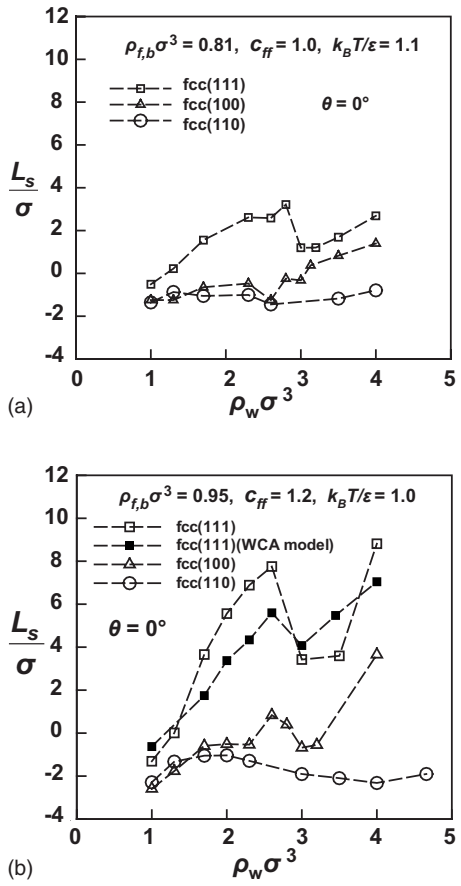

FIG. 8. Variations of slip length in Couette flow at $\theta=0°$, $k_BT/\varepsilon=1.1$, and $\rho_{f,b}\sigma^3=0.95$ with the wall density and lattice plane. (a) Usual LJ fluid ($c_{ff}=1.0$) and (b) cohesive LJ fluid ($c_{ff}=1.2$). Simulations with WCA model are presented for comparison.

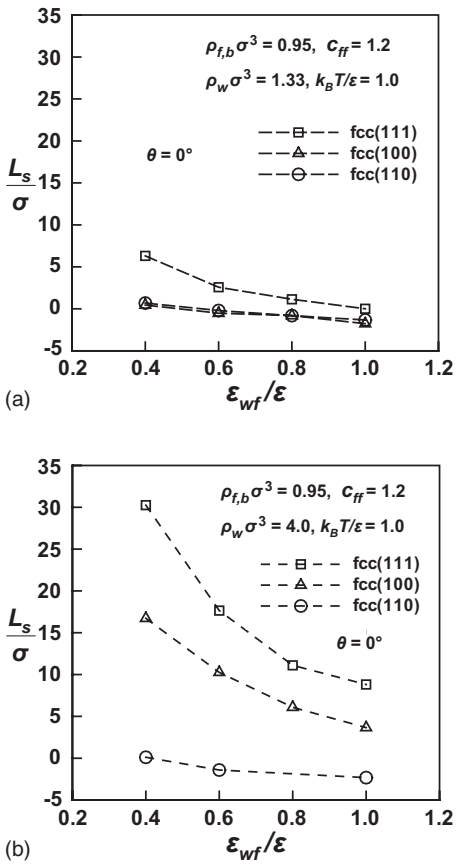

FIG. 9. Variation of slip length with the interaction parameter $\varepsilon_{wf}/\varepsilon$ for LJ fluid of $c_{ff}=1.2$ and $\rho_{f,b}\sigma^3=0.95$ at $\theta=0°$, $k_BT/\varepsilon=1.0$, and the wall density of $\rho_w\sigma^3=$(a) 1.3 and (b) 4.0.

cale flows. The slip length L_s, as a measure of fluid slippage, is defined in Navier's slip formula $U_S=L_S(dU/dn)_w$, where U_S stands for the slip velocity and $(dU/dn)_w$ for the wall velocity gradient in the normal direction (n). The effects of wall and fluid properties and the wall-fluid interaction parameters on the slip length are considered. In Fig. 8, the effects of wall density variation on the slip length in the Couette flow are presented. The slip length is obtained by linear fit of the velocity data but, to reduce the statistical noise, with the data in near-wall regions of thickness 1.5σ excluded. The multilayer-sticking phenomenon is characterized by a negative slip length. In this situation, the fluid particles in a thin region adjacent to the solid wall are immobile. Minimum slip length may occur when the wall and fluid densities are low and commensurate. As mentioned in a previous study [12], the slip length varies with wall density in a nonmonotonic manner. A local minimum appears when the wall density $\rho_w\sigma^3$ lies in a range around 3. Generally speaking, a smooth and/or high-density wall tends to generate a large slip length. This nonmonotonic dependence of wall density is inferred as a consequence of the complicated wall-fluid interaction mechanisms mentioned in the discussion of the results shown in Fig. 5. To explore the slip length correlation more extensively, Couette flows of cohesive fluids ($c_{ff}=1.2$) with bulk fluid density $\rho_{f,b}\sigma^3=0.95$ are studied, and the MD results with variations in wall density are presented in Fig. 8(b). The data shown in both figures have similar qualitative trends. For the rougher channel wall of fcc (110) with flow orientation angle $\theta=0°$, mild changes in slip length are presented; whereas a nonmonotonic nature appears in the cases of smoother walls, i.e., fcc (111) and (100). To further examine the slip length variation, simulations for the cases of fcc (111) using the WCA model ($c_{ff}=0$) are performed. It is interesting to note that the nonmonotonic behavior appears in the simulations with $c_{ff}=0$, 1.0, and 1.2, which correspond to fluids without interparticle attraction force, normal LJ fluids, and more cohesive LJ fluids, respectively. This observation implies that the attraction between fluid particles is irrelevant to the mechanism of this anomalous behavior of wall-density dependence.

The interaction energy parameter ε_{wf} is also one of the influential factors on the wall-fluid interaction. A strong interaction potential enhances the wall-fluid exchange of momentum and energy and tends to alleviate the discontinuity at the interface. Therefore, the slip length decreases monotonically with increasing ε_{wf} as the MD predictions show in Fig. 9. There, variations of the slip length with the interaction parameter ε_{wf} at the wall densities $\rho_w\sigma^3=1.33$ and $\rho_w\sigma^3=4.0$ are plotted in Figs. 9(a) and 9(b), respectively. In all cases considered, the lattice plane (111) always results in the largest fluid slippage among the three surfaces. For the lower wall density considered in Fig. 9(a), since the bulk fluid den-

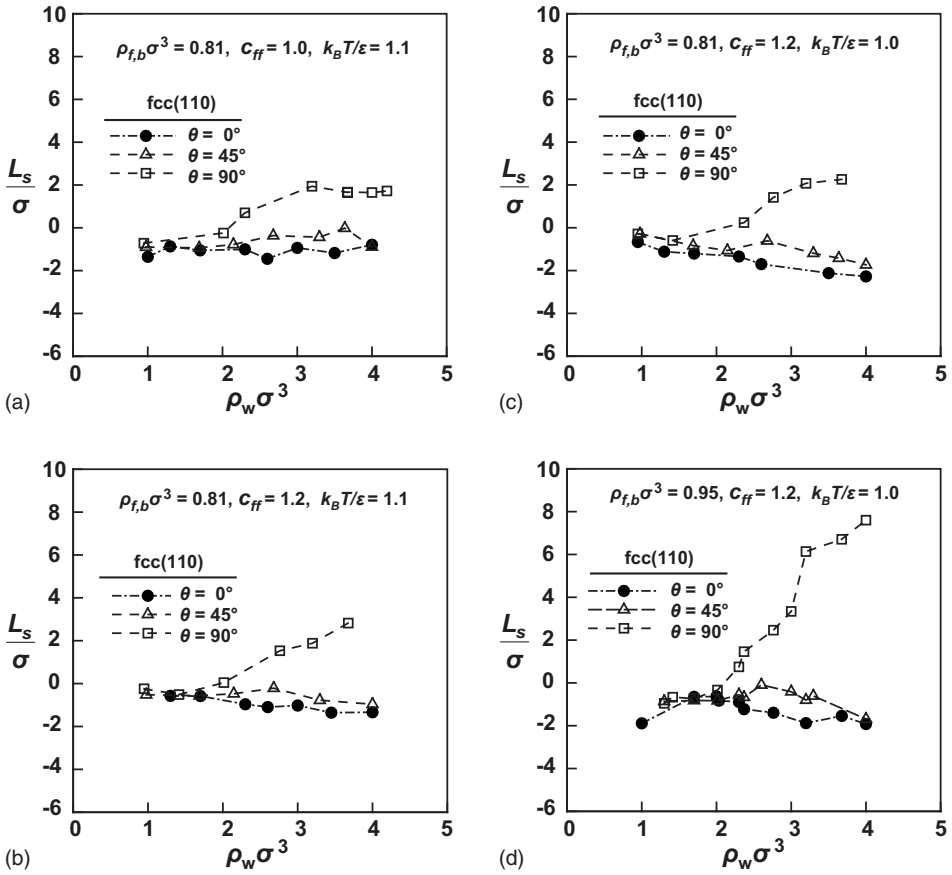

FIG. 10. Variations of slip length with wall density and flow orientation in a nanochannel with fcc (110) wall surface.

sity $\rho_{f,b}\sigma^3=0.95$ is close to $\rho_w\sigma^3=1.33$, the strong wall-fluid interaction results in multilayer sticking phenomenon or a negative slip length. As the wall density increases up to $\rho_w\sigma^3=4.0$, the slip length is generally increased, as shown in Fig. 9(b). The behavior of the plane fcc (110) is an exception. Compared with the data shown in Fig. 9(a), the slip length at $\rho_w\sigma^3=4.0$ does not increase but decreases. This different behavior can be elucidated with the curve for fcc (110) shown in Fig. 8(b).

The orientation of the flow over solid surfaces may have significant impact on interfacial phenomena. The flow orientation is characterized by the flow angle defined in Fig. 1. Among the three lattice planes considered, fcc (110) is the most anisotropic and rough one, and is employed to examine the flow orientation effects in Fig. 10. The three angles 0°, 45°, and 90° designate the situations of flow across the surface molecular trenches, the flow over the surface at the angle 45° with the atomistic trenches, and the fluid flow along the trenches, respectively. Figure 10(a) shows the MD results for L_s/σ versus $\rho_w\sigma^3$ for the usual LJ fluid with $\rho_{f,b}\sigma^3=0.81$, $c_{ff}=1.0$, and $k_BT/\varepsilon=1.1$. With the above as the baseline cases c_{ff} is changed to 1.2 in Fig. 10(b), then k_BT/ε is changed to 1.0 in Fig. 10(c), and finally, in Fig, 10(d), the fluid bulk density $\rho_{f,b}\sigma^3$ is further changed from 0.81 to 0.95. Generally speaking, for the lattice plane fcc (110), the results in Fig. 10 demonstrate that the fluid slippage is strongly influenced by the flow orientation as well as the wall density, and the slip length increases monotonically with the flow orientation angle (θ). The slip length at flow angle $\theta=90°$ is largest; while the slip lengths at the flow angles $\theta=0°$ and 45° are lower, and these two flow configurations have quite similar characteristics. The fluid slippage is more pronounced with high wall density, or $\rho_w\sigma^3>2$. The results also show that the fluid slippage at the orientation angle $\theta=90°$ can be highly enhanced by raising the fluid bulk density $\rho_{f,b}\sigma^3$ up to 0.95.

D. Similarity of interfacial phenomena and poiseuille flow rates

Figure 11 presents variations in slip length under the influence of wall density, lattice plane, and flow orientation. In particular, this section emphasizes the comparison of fluid slippage phenomena in Couette and Poiseuille flows, and explores the possible similarity between the interfacial phenomena in nanochannel flows. In general, all the data demonstrate similarity in Couette and Poiseuille flows, both qualitatively and quantitatively. For a detailed exploration, Fig. 11(a) shows that this similar trend exists for the more cohesive LJ fluid flow over various lattice planes at the orientation angle $\theta=0°$. In Fig. 11(b), the results for the plane (110) with flow orientation angles $\theta=0°$, 45°, and 90° are presented. With respect to the variations of wall density, the results in Figs. 11(a) and 11(b) show quite good agreement of the slip lengths in the two flows at various conditions.

With focus on the influence of the flow orientation angle, Fig. 11(c) plots the slip length correlations for both the Couette and Poiseuille flows. At flow orientation angles between 0° and 45°, the slip length over the lattice plane (111) is the largest among the three surfaces, and varies in a periodic

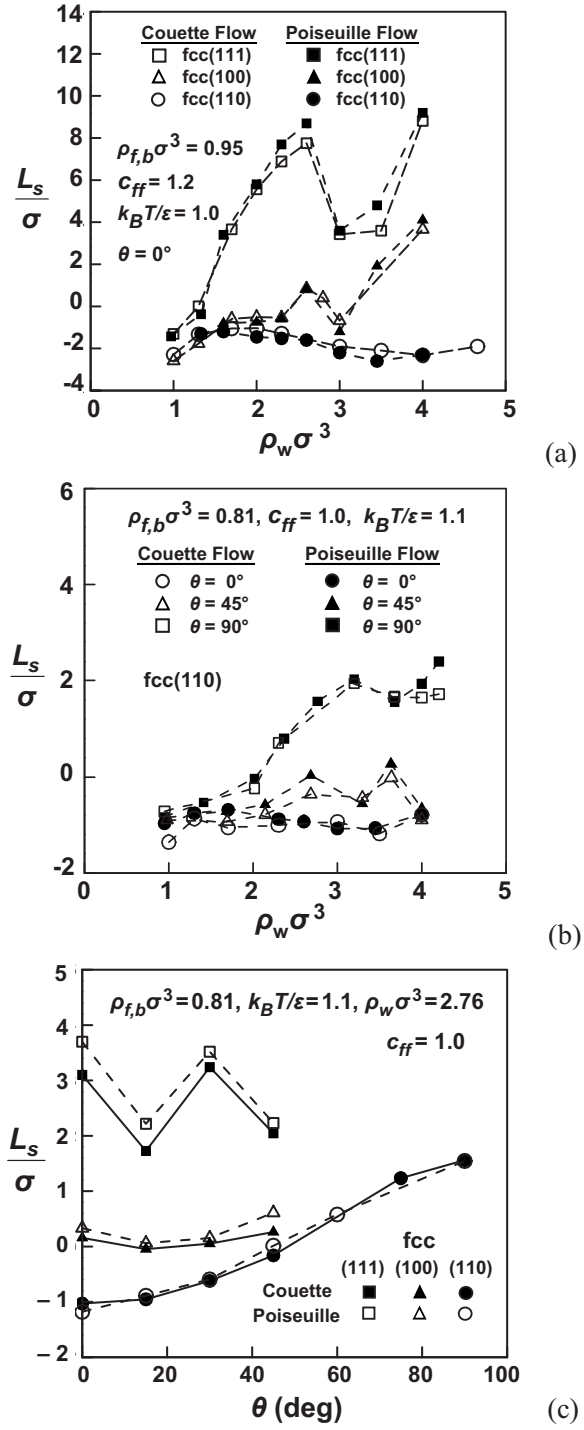

FIG. 11. Slip lengths (L_s/σ) in Couette and Poiseuille flows versus $\rho_w\sigma^3$ with various wall densities and lattice planes in (a) more cohesive LJ fluids and (b) the usual LJ fluids. (c) L_s/σ versus flow angle θ with various lattice planes.

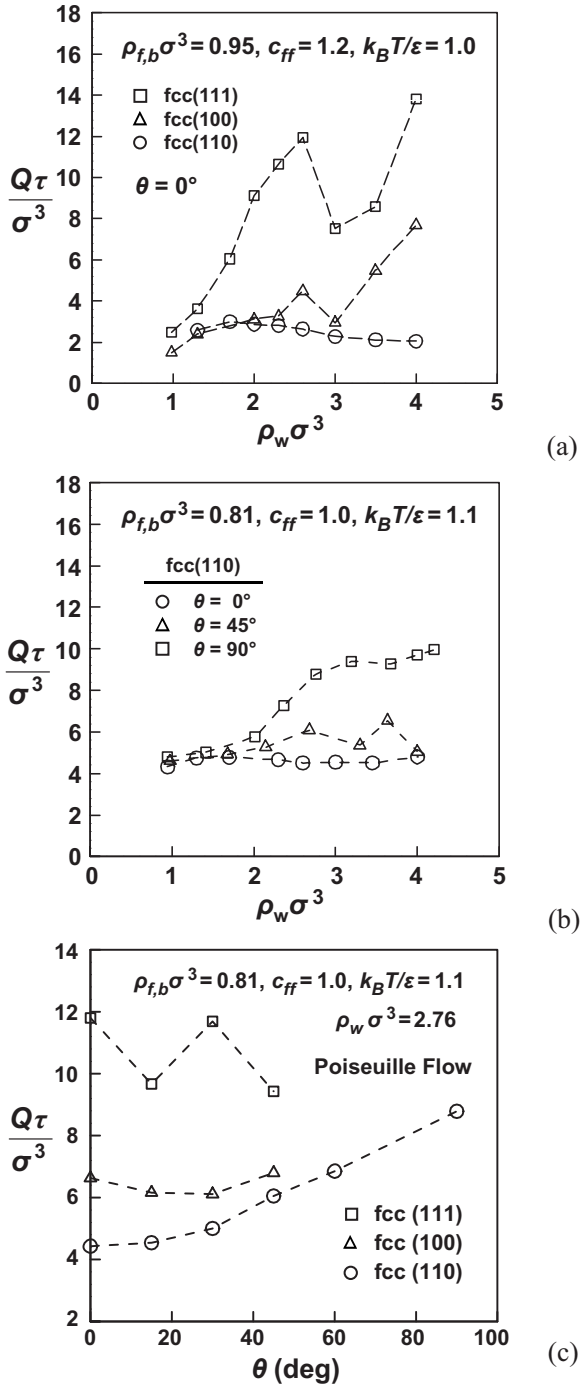

FIG. 12. (a) Slip lengths in Couette and Poiseuille flows; (b) Poiseuille flow rates of usual LJ fluid with various flow orientations at solid-fluid interface of fcc (110); (c) comparison of flow rate correlations with flow angles for various lattice planes.

pattern corresponding to the symmetry nature of the first-layer lattice plane. The slip length for the surface (100) is smaller than that for (111), and has the smallest sensitivity to the change of flow angle. As to the slip length for the surface (110), it is the smallest among the three and has a monotonic variation with the flow angle. With the Couette flow data as illustrative examples, it is found that the slip length at the interface of the wall surface (110) presents an ascending trend with increases in flow orientation angle (θ). At $\theta=0°$, the slip length is negative ($L_s/\sigma=-1.03$), which means that the flow over the surface has to cross over the trenches formed by the wall surface atoms. Fluid particles may be trapped in the trenches, and multilayer sticking occurs. As the flow angle changes to $\theta=45°$, the cross-trench phenomenon still appears but becomes moderate and the negative

TABLE I. Variations of slip length and flow rate in nanochannel flows with variation in wall density, surface, and flow orientation. LJ fluids (c_{ff}=1.0) at bulk fluid density $\rho_{f,b}\sigma^3$=0.81 and temperature k_BT/ε =1.1 are considered.

Surface orientation	Flow orientation θ (deg)	Wall density $\rho_w\sigma^3$	Energy scale $\varepsilon_{wf}/\varepsilon$	Length scale σ_{wf}/σ	Slip length L_S/σ	Flow rate $Q\tau/\sigma^3$
			Couette flow			
fcc (111)	0	4.0	0.6	0.75	4.8	
	0	3.0	1.0	0.857	1.25	
	15	3.0	1.0	0.857	1.76	
	30	3.0	1.0	0.857	2.13	
	45	3.0	1.0	0.857	2.25	
	0	2.76	1.0	0.867	3.1	
	15	2.76	1.0	0.867	1.726	
	30	2.76	1.0	0.867	3.241	
	45	2.76	1.0	0.867	2.045	
	90	2.76	1.0	0.867	3.45	
	0	2.6	1.0	0.873	2.588	
	15	2.6	1.0	0.873	2.474	
	30	2.6	1.0	0.873	2.275	
fcc (100)	0	4.0	0.6	0.75	2.6	
	0	3.0	1.0	0.857	−0.446	
	15	3.0	1.0	0.857	0.138	
	30	3.0	1.0	0.857	0.157	
	45	3.0	1.0	0.857	−0.332	
	0	2.76	1.0	0.867	0.1565	
	30	2.76	1.0	0.867	−0.0482	
	45	2.76	1.0	0.867	0.0518	
	90	2.76	1.0	0.867	0.2622	
	0	2.6	1.0	0.873	0.466	
	15	2.6	1.0	0.873	−0.087	
	30	2.6	1.0	0.873	0.207	
	45	2.6	1.0	0.873	−0.178	
fcc (110)	0	4.0	0.6	0.75	−0.4	
	0	3.0	1.0	0.857	−1.037	
	45	3.3	1.0	0.846	−0.438	
	70	3.2	1.0	0.85	0.634	
	90	3.2	1.0	0.85	1.942	
	0	2.76	1.0	0.867	−1.03	
	15	2.76	1.0	0.867	−0.954	
	30	2.76	1.0	0.867	−0.621	
	45	2.76	1.0	0.867	−0.1667	
	60	2.76	1.0	0.867	0.2765	
	75	2.76	1.0	0.867	1.239	
	90	2.76	1.0	0.867	1.56	
	0	2.6	1.0	0.873	−1.36	
	15	2.6	1.0	0.873	−0.986	
	30	2.6	1.0	0.873	−0.812	
	45	2.6	1.0	0.873	−0.42	
	90	2.6	1.0	0.873	−0.339	
			Poiseuille flow			
fcc (111)	0	4.0	0.6	0.75	5.2	13.48
	0	3.0	1.0	0.857	1.46	8.14
	15	3.0	1.0	0.857	1.6	8.84

TABLE I. (*Continued.*)

Surface orientation	Flow orientation θ (deg)	Wall density $\rho_w\sigma^3$	Energy scale $\varepsilon_{wf}/\varepsilon$	Length scale σ_{wf}/σ	Slip length L_S/σ	Flow rate $Q\tau/\sigma^3$
	30	3.0	1.0	0.857	1.88	9.1
	45	3.0	1.0	0.857	2.24	9.52
	0	2.76	1.0	0.867	3.7	11.801
	15	2.76	1.0	0.867	2.21	9.669
	30	2.76	1.0	0.867	3.52	11.69
	45	2.76	1.0	0.867	2.12	9.43
	90	2.76	1.0	0.867	3.66	11.77
	0	2.6	1.0	0.873	3.057	10.78
	15	2.6	1.0	0.873	2.77	10.03
	30	2.6	1.0	0.873	3.03	10.77
fcc (100)	0	4.0	0.6	0.75	2.8	9.42
	0	3.0	1.0	0.857	−0.233	5.82
	15	3.0	1.0	0.857	0.552	6.6
	30	3.0	1.0	0.857	0.5539	6.76
	45	3.0	1.0	0.857	−0.128	5.79
	0	2.76	1.0	0.867	0.332	6.63
	15	2.76	1.0	0.867	0.0598	6.164
	30	2.76	1.0	0.867	0.154	6.112
	45	2.76	1.0	0.867	0.609	6.799
	0	2.6	1.0	0.873	0.3125	5.789
	15	2.6	1.0	0.873	0.213	6.606
	30	2.6	1.0	0.873	0.353	6.761
	45	2.6	1.0	0.873	0.473	5.818
fcc (110)	0	4.0	0.6	0.75	−0.4	5.12
	0	3.0	1.0	0.857	−1.074	4.56
	45	3.3	1.0	0.846	−0.562	5.36
	70	3.2	1.0	0.85	0.943	7.5
	90	3.2	1.0	0.85	2.234	9.4
	0	2.76	1.0	0.867	−1.18	4.429
	15	2.76	1.0	0.867	−0.888	4.542
	30	2.76	1.0	0.867	−0.5936	5.003
	45	2.76	1.0	0.867	0.014	6.052
	60	2.76	1.0	0.867	0.5789	6.852
	90	2.76	1.0	0.867	1.545	8.787
	0	2.6	1.0	0.873	−1.035	4.458
	15	2.6	1.0	0.873	−0.831	4.569
	30	2.6	1.0	0.873	−0.593	5.3
	45	2.6	1.0	0.873	−0.272	5.78
	90	2.6	1.0	0.873	0.124	6.328

slip length is reduced ($L_s/\sigma=-0.1667$). The slip length becomes positive, $L_s/\sigma=0.2765$, as θ further increases to 60°, and $L_s/\sigma=1.239$ at $\theta=75°$. At the flow angle $\theta=90°$, the flow direction is parallel to the atomistic trenches, and the fluid particles can migrate over the surface smoothly along the flow direction. At this flow orientation, the slip length reaches a maximum value, $L_s/\sigma=1.58$.

Corresponding to the fluid slippage disclosed in Fig. 11, the Poiseuille flow rates shown in Fig. 12 manifest the effects of the wall density, the lattice plane, and the flow orientation in a similar trend. It seems reasonable, since the velocity profile of the Poiseuille flow in a nanochannel can be described by the continuum hydrodynamics valid in the off-wall region, but with the slip boundary condition, viz.,

$$U(Z)=\frac{f_p\rho}{2\mu}\left[\left(\frac{H}{2}\right)^2-\left(Z-\frac{H}{2}\right)^2\right]+U_S. \tag{4}$$

The flow rate evaluated by integrating the above velocity profile definitely increase with slip length.

The data presented in Figs. 11(c) and 12(c) reveal that the hydrodynamics in nanochannel flows are quite distinct for

various lattice planes. For the plane (111), the velocity profiles at $\theta=15°$ and 45° are very close, as also are those at $\theta=0°$ and 30°. These somewhat periodic variations reflect the symmetry of the influences from the surface atoms. For the channel wall of plane (100), the hydrodynamics at flow orientation angles of $0° \leqslant \theta \leqslant 45°$ change slightly. It is reasonably speculated that, relative to the pattern of the surface atoms, the contributions of the second and third layers may not be in phase, and thus tend to reduce the differences in the wall-fluid interactions at different flow angles. For the most anisotropic and roughened surface, fcc (110), noticeable and monotonic variations with flow orientation angles between 0° and 90° are observed. Some important digital data of the present MD simulations about the slip lengths and flow rates are listed in Table I.

IV. CONCLUDING REMARKS

In the present MD study, we demonstrate that interfacial characteristics, including density layering, fluid slippage, and channel flow rate, are significantly influenced by the surface orientation, flow orientation, wall and fluid densities, and molecular interaction parameters. In nanochannel flows, solid walls of the same crystal lattice but with different surface orientations will lead to noticeable changes in interfacial characteristics, including density layering and fluid slippage, and thus the flow rate in a nanochannel. For the three surface orientations studied in the present work, the MD results reveal that the flow orientation with respect to the wall lattice structure has very remarkable influence on the fluid slippage, and in turn the velocity profile and flow rate. The influence of the surface and flow orientations disclosed in the present study is significant in understanding nanofluidics, as well as in future applications to accurate flow rate control at nanoscales. Based on the present MD simulations, the following significant physical findings can be summarized.

(1) With increasing wall-fluid interaction potential ε_{wf} and/or wall density $\rho_w\sigma^3$, the density layering can be enhanced. The density peak value for fcc (110) increases with wall density, whereas nonmonotonic variations of the density peak values over the surfaces fcc (111) and fcc (100) appear with the wall density parameter $\rho_w\sigma^3$ in a range around 3, due to complicated wall-fluid interaction mechanisms related to wall molecular structure, and the interaction distance of fluid and wall molecules in multilayers.

(2) Among the three surface orientations, the slip length for the smoothest wall, fcc (111), is largest, especially at a high wall density. The surface fcc (110) is the most roughened and anisotropic, and has lower and usually negative slip length. In addition, nonmonotonic variation of slip length with increasing wall density for the two smoother walls, fcc (111) and fcc (100), is similar to the variations of peak values in the density layering phenomenon.

(3) By employing the wall surface fcc (110) as a model, it is disclosed that flow along the molecular trenches of the surface leads to the largest slip length, and flow across the trenches presents the smallest slippage. The slip flow is more pronounced with high wall density or $\rho_w\sigma^3 > 2$.

(4) With the parameter ranges considered in the present study, the MD predictions of slip length in Couette and Poiseuille flows have very similar qualitative and quantitative features, which implies the possibility of universality of the interfacial characteristics in nanochannel flows.

(5) The most striking results of the present study are the effects of flow orientations on the nanochannel flows. The present MD simulations disclose that the influences of the flow orientation are quite distinct for various lattice planes, i.e., periodic variation with flow angle for the wall lattice plane (111), the smallest sensitivity to the flow angle for the plane (100), and monotonic variation for the plane (110).

(6) The fluid slippage and the flow rate will be different if the channel walls are of different lattice planes and/or the fluid flows over the wall at a different orientation angle. Therefore, even if the nanochannels are fabricated using the same material (fixed wall density) of a fixed crystal structure, e.g., fcc, the flow rate may be different. These influences of surface and flow orientations disclosed in this work are of significance to the understanding of nanofluidic characteristics, as well as to future applications in various disciplines, where an accurate nanoscale flow rate control is necessary.

ACKNOWLEDGMENT

Financial support from National Science Council of the Republic of China (Taiwan) through Grant No. NSC-95-2221-E-035-052-MY3 is acknowledged.

[1] U. Heinbuch and J. Fischer, Phys. Rev. A **40**, 1144 (1998).
[2] P. A. Thompson and M. O. Robbins, Phys. Rev. A **41**, 6830 (1990).
[3] P. A. Thompson and S. M. Troian, Nature (London) **389**, 360 (1997).
[4] A. Jabbarzadeh, J. D. Atkinson, and R. I. Tanner, J. Chem. Phys. **110**, 2612 (1999).
[5] J.-L. Barrat and L. Bocquet, Phys. Rev. Lett. **82**, 4671 (1999).
[6] J.-L. Barrat and L. Bocquet, Faraday Discuss. **112**, 119 (1999).
[7] C. Cotton-Bizonne, J. L. Barrat, L. Bocquet, and E. Charlaix, Phys. Rev. Lett. **94**, 056102 (2005).
[8] N. V. Priezjev, A. A. Darhuber, and S. M. Troian, Phys. Rev. E **71**, 041608 (2005).
[9] M. Cieplak, J. Koplik, and J. R. Banavar, Phys. Rev. Lett. **96**, 114502 (2006).
[10] C. Y. Soong, S. H. Wang, and P. Y. Tzeng, Phys. FluidsPhys. Fluids **16**, 2814 (2004).
[11] C. Cotton-Bizonne, J. L. Barrat, L. Bocquet, and E. Charlaix, Nat. Mater. **2**, 237 (2003).
[12] D. Kim and E. Darve, Phys. Rev. E **73**, 051203 (2006).
[13] R. Qiao, Microfluid. Nanofluid. **3**, 33 (2007).
[14] M. Sbragaglia, R. Benzi, L. Biferale, S. Succi, and F. Toschi, Phys. Rev. Lett. **97**, 204503 (2006).
[15] W. D. Kaplan and Y. Kauffmann, Annu. Rev. Mater. Res. **36**,

1 (2006).
[16] J. Q. Broughton and G. H. Gilmer, J. Chem. Phys. **79**, 5095 (1983); **84**, 5741 (1986).
[17] T. M. Galea and P. Attard, Langmuir **20**, 3477 (2004).
[18] J. D. Weeks, D. Chandler, and H. C. Andersen, J. Chem. Phys. **54**, 5237 (1971).
[19] R. Khare, J. Pablo, and A. Yethiraj, J. Chem. Phys. **107**, 2589 (1997).
[20] D. J. Evans and B. L. Holian, J. Chem. Phys. **83**, 4069 (1985).